Rate coefficient for the reaction H+O2→OH+O: Results at high temperatures, 2000 to 5300 K

Hong Du and Jan P. Hessler

Citation: J. Chem. Phys. **96**, 1077 (1992); doi: 10.1063/1.462194
View online: http://dx.doi.org/10.1063/1.462194
View Table of Contents: http://jcp.aip.org/resource/1/JCPSA6/v96/i2
Published by the American Institute of Physics.

Rate coefficient for the reaction $H+O_2 \rightarrow OH+O$: Results at high temperatures, 2000 to 5300 K

Hong Du and Jan P. Hessler
Gas Phase Chemical Dynamics Group, Chemistry Division, Argonne National Laboratory, 9700 South Cass Avenue, Argonne, Illinois 60439

(Received 12 June 1991; accepted 7 October 1991)

The tunable-laser flash-absorption technique has been used to study the high-temperature behavior of the reaction $H + O_2 \rightarrow OH + O$ by monitoring the absorption of the hydroxyl radical. Sensitivity analysis of a detailed reaction mechanism shows that for fuel rich mixtures only two reactions are sensitive when hydroxyl is monitored: $H_2 + M \rightarrow 2H + M$ and $H + O_2 \rightarrow OH + O$. Rate coefficients for these reactions have been determined by least-squares analysis of measured absorption profiles. For the rate of dissociation of H_2 in krypton we obtain

$$k_1(T) = (8.86 \pm 0.88) \times 10^{-10} \exp[-48321/T(K)] \text{ cm}^3 \text{ s}^{-1}$$

from 3450 to 5300 K. For the $H + O_2$ reaction we combined our results with previous low temperature measurements and recommend

$$k_2(T) = (1.62 \pm 0.12) \times 10^{-10} \exp[-(7474 \pm 122)/T(K)] \text{ cm}^3 \text{ s}^{-1}$$

from 960 to 5300 K. The uncertainties are at the 95% confidence level. Measured cross sections for rotational and vibrational energy transfer in O_2 and OH have been used to show that relaxation effects do not influence the results. We compare our results to recent trajectory calculations. In addition, we calculate the rate of the reverse reaction, $OH + O \rightarrow H + O_2$, and compare it to trajectory and statistical adiabatic channel calculations. Finally, we point out that the first excited surface of the hydroperoxyl radical, $^2A'$, which correlates with $H(^2S) + O_2(^1\Delta_g)$, may be needed to explain very high temperature results.

I. INTRODUCTION

The reaction between atomic hydrogen and molecular oxygen, $H + O_2 \rightleftarrows HO_2^* \rightarrow OH + O$, is one of the most important reactions in gas-phase combustion. For example, it is important in the oxidation of H_2,[1] controls the chain branching in the oxidation mechanism for all hydrocarbon fuels,[2] and is the beginning reaction in a hierarchical scheme for modeling combustion reactions in flowing systems.[3] Recent reviews of the status of the rate of this reaction have been carried out by Baulch *et al.*,[4] Cohen and Westberg,[5] and Warnatz.[6] In spite of the importance of this reaction, there is a controversy over the temperature dependence of the rate coefficient at high temperatures. In 1973 Schott[7] deduced the temporal behavior of the oxygen concentration from measurements of the chemiluminescence from O–CO recombination (1250 to 2500 K) and found non-Arrhenius behavior of the form $T^{-0.907}$ and an activation energy, $E/k = 8369$ K. This result was explained by Miller,[8] who performed quasiclassical trajectory and quasiclassical quantum mechanical threshold calculations on an analytical representation of the Melius–Blint[9] *ab initio* surface and found that the negative curvature was due to a dynamic effect associated with a light particle reacting with two heavy particles. In 1985, Frank and Just[10] used atomic resonance absorption spectrophotometry[11] to simultaneously measure atomic oxygen and hydrogen (1700 to 2500 K) and found Arrhenius behavior with an activation energy, $E/k = 8691$ K. This behavior is consistent with statistical adiabatic channel calculations on a simple one-dimensional potential surface.[12] The controversy is focused on the temperature dependence of the preexponential factor. In dynamic terms, at issue is the relative importance of statistical vs nonstatistical recrossing of the transition state.[13] Statistical recrossing arises from the ratio of probabilities for the dissociation of the intermediate complex, HO_2^*, into the forward and reverse channels, and is not important except at extremely high temperatures. Nonstatistical recrossing occurs when a significant fraction of the trajectories entering the strong interaction region do not yield products even at very low temperatures.

Since 1988, five groups have reported measurements of the rate coefficient of this reaction at the high temperatures produced by shock tube techniques. Three have used the continuous-wave laser technique developed at Stanford[14] to monitor the concentration of hydroxyl[15–17] and the other two[18,19] have used flash photolysis[20] to produce hydrogen atoms, and follow their decay with atomic resonance absorption spectrophotometry. The experimental results agree below 1600 K, however, the temperature dependence of the pre-exponential factors ranges from $T^{-0.927}$ to $T^{2.0}$. Because of the different temperature dependent prefactors, the results diverge significantly at high temperatures. For example, at 2600 K the extreme results differ by a factor of 2.2, and when extrapolated to 5000 K they differ by a factor of 7.4. Clearly, measurements up to 5000 K should help to resolve this controversy, provide a reliable phenomenological

rate coefficient, and significantly extend the data base for the reaction so that theoretical calculations of thermal rate coefficients may be tested against experimental results.

In this paper, we report measurements from 2000 to 5300 K performed with our new tunable-laser flash-absorption technique[21] from which rate coefficients are determined by nonlinear least-squares analysis of hydroxyl concentrations calculated from a complete reaction mechanism. In addition, above 3000 K an incubation period is observed and the rate of dissociation of H_2 is determined. We present calculations of rotational and vibrational relaxation rates to show that relaxation processes do not affect our results. By extending the temperature range of the measurements by 2000 K and combining our results with previous low temperature results, we conclude that the rate coefficient for the $H + O_2$ reaction follows a simple Arrhenius expression from 960 to 5300 K. Therefore, the preexponential factor may be treated as being independent of temperature. We compare both forward and reverse rate coefficients to recent theoretical calculations. Statistical adiabatic channel model calculations on a one-dimensional representation of both the ground and excited electronic surfaces overestimate the $OH + O$ rate coefficient. We cannot draw any firm conclusions from current trajectory calculations. Finally, we point out the need to include the first excited surface of the hydroperoxyl radical and the $H(^2S) + O_2(^1\Delta_g)$ channel into calculations of the reverse reaction at high temperatures, $T \geqslant 1000$ K.

This paper is organized as follows. In Sec. II, we briefly describe the tunable-laser flash-absorption technique, point out that the high frequency response of the technique allows us to perform measurements at very high temperatures, and report the experimental details of the shock tube and sample preparation apparatus. The reaction mechanism and least-squares method used to evaluate rate coefficients are described in Sec. III. In Sec. IV, we present our results: new measurements for the dissociation rate of H_2 in krypton, and, of course, the temperature dependence of the rate coefficient for the $H + O_2 \rightarrow OH + O$ reaction. In Sec. V, we discuss the implications of our results, including an analysis of $OH + O \rightarrow H + O_2$, the reverse of the titled reaction, and present our conclusions.

II. EXPERIMENTAL DETAILS

The kinetic behavior of the H_2/O_2 system was monitored by measuring the concentration of the hydroxyl radical immediately behind a shock front by using the tunable-laser flash-absorption technique developed in this laboratory.[21] Figure 1 shows a schematic of the experimental setup. Briefly, light from a high-resolution, pulsed, dye-laser system is tuned to the center of a strong absorption line of the species of interest. For hydroxyl, we used the ${}^{Q}Q_{11}(13/2)$ $[{}^{\Delta N}\Delta J_{F'F''}(J'')$ notation] transition of the (0,0) band at 32 381 cm^{-1}. This light beam is focused to produce a relatively long and uniform spatial distribution along the axis of the shock tube and is timed to tranverse the shock tube when the shock front is located in front of a linear-array detector. This detector measures the transmitted

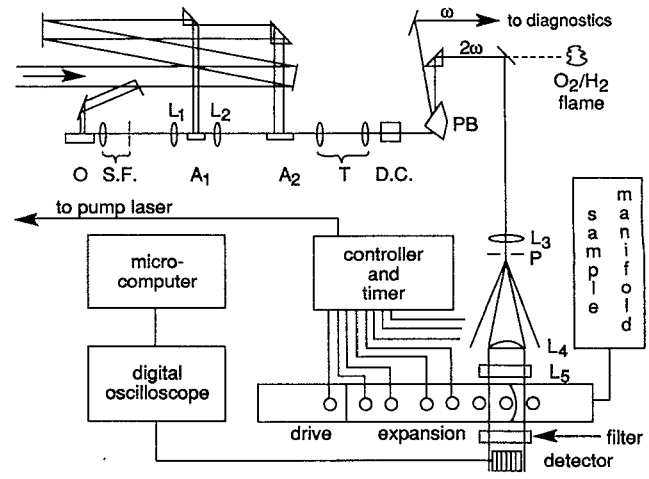

FIG. 1. Schematic diagram of the experimental apparatus.

energy as a function of distance along the axis of the shock tube. When two independent light pulses are sampled, one with a shock front and the other without, the absorption coefficient as a function of the distance behind the shock front can be calculated. If the absorbing species is in thermodynamic equilibrium with the bath gas, this absorption coefficient is proportional to the concentration of the absorbing species. When enough is known about the parameters which describe the absorption process, the concentration can be calculated absolutely. We have already described[21] the basic principles of the technique, the laser system, and the linear-array detector system used to perform these measurements. Here we only present details of the shock tube and sample preparation system which have a direct bearing on our measurements.

One advantage of the flash-absorption technique is the very high effective bandwidth of the detection system. This bandwidth determines the maximum rate of change of concentration that can be accurately measured. The flash-absorption technique acquires spatial information and converts it to temporal information through the velocity of the shock front. Therefore, the bandwidth is determined by the width of an element on the array detector (25.4 μm) and the duration of the light pulse (16 ns). Our effective bandwidth is greater than 60 MHz. For comparison, the bandwidth for both the continuous-wave laser technique and atomic-resonance absorption spectrophotometry is determined by the RC (resistance capacitance) time constant of the detection system. A typical 3 dB bandwidth for monitoring a continuous-wave laser system is 150 kHz.[16] The larger bandwidth of the flash-absorption technique allows us to measure accurately very rapid changes in concentration. Therefore, we can perform measurements at very high temperatures where the rates of the reactions are very fast.

Because the flash-absorption technique is sensitive, we constructed a relatively small shock tube. Special care was taken to insure high purity. The shock tube consists of a 25.4 mm diameter honed and electropolished, stainless steel tube with a 2.0 m long expansion section and a 0.65 m long drive

section. The expansion section was evacuated with a Seiko–Seiki 300 ℓs^{-1} turbomolecular pump equipped with magnetic levitation bearings. The ultimate pressure of the system was 5×10^{-7} Torr. Experiments were performed with turnaround times of approximately 30 min with typical evacuated pressures less than 1×10^{-6} Torr. In addition, a residual-gas analyzer (RGA) was attached to the system so a mass spectrum of the residual gases could be measured before each shock. The driver and expansion sections were separated by several 0.001 in. thick mylar diaphragms. Helium (ultrahigh purity, 99.999%) was used as the driver gas and was rapidly introduced into the drive section until the diaphragms burst.

Gas samples were prepared by the partial pressure method in a baked, electropolished, 3 ℓ, stainless-steel tank. Ultimately, this tank and the entire sample manifold were evacuated with the same turbomolecular pump used to evacuate the expansion section of the shock tube. Prior to making a sample, the system was evacuated to 5×10^{-7} Torr and the composition of the residual gas was measured with the RGA. Typically, hydrocarbons were less than 10^{-9} Torr, $H_2O\sim8\times10^{-8}$ Torr, $O_2\sim1\times10^{-8}$ Torr, and $N_2/CO\sim4\times10^{-8}$ Torr. The dominant gas was either argon or krypton. Two MKS Baratron capacitive manometers, 10 and 10 000 Torr full scale, were used to measure the reactant and buffer gas pressures. The most concentrated sample contained ~6 Torr of O_2, ~60 Torr of H_2, and ~1500 Torr of Kr. The accuracy of these pressure measurements is $\pm0.5\%$. Such a sample could be used for many shocks. To insure that the gases were turbulently mixed, the rare gas was introduced rapidly into the mixing cell by a series of short bursts. The following gases were used in sample mixtures: O_2 from Matheson, impurities: CH_4, CO, and CO_2 all <0.1 ppm, nitrous oxide <1 ppm, and $H_2O<1.6$ ppm; H_2 from Matheson, impurities: CO_2, CO, and CH_4 all <0.1 ppm, O_2 and Ar both <0.5 ppm, $N_2<1$ ppm, and $H_2O<2$ ppm; Ar from Airco, impurities: O_2, CO, CO_2, total hydrocarbons, and H_2O all <1 ppm, $H_2<2$ ppm, and $N_2<4$ ppm; and Kr from MG Industries Gas Products, impurities: O_2, H_2O, and total hydrocarbons all <1 ppm, $N_2<5$ ppm, and $H_2<10$ ppm. All gases were used without further purification. Samples were introduced into the experimental section from the end of the shock tube nearer the detector. A Fluid Precision pressure transducer, type 120 with a full scale range of 100 Torr, was used to measure the initial pressure in the shock tube and a thermocouple was used to measure the initial temperature. The uncertainty for these pressure measurements is $\pm(0.15\%+0.005$ Torr). Although the thermocouple can be read to ±0.1 K, we assume the uncertainty of the temperature of the gas within the shock tube is ±0.5 K. Shock speeds were measured with a series of five barium titanite pressure transducers (International Transducers, model PK14-12) mounted at 100 mm intervals along the expansion section. The signals from the transducers were differentiated, amplified, and used to start and stop a 10 MHz counter driven by a crystal oscillator, Dale model XO-43B, with a frequency stability of $\pm0.01\%$. The measured time intervals were fit to a quadratic equation. The transducer located above the center of the detector was used for the origin, thereby minimizing any correlation between the coefficients of the quadratic equation. The uncertainty in the shock speed is less than 0.2% at the 95% confidence level. Over the 300 mm interval preceeding the observation zone the speed of the shock front decreased by less than 0.6%.

Because we used the least-squares method, we are able to extract rate coefficients from absorption profiles with relatively small signal-to-noise ratios. Therefore, we have chosen to perform experiments with initial concentrations of hydrogen and oxygen which produce profiles with the maximum absorption between 5 and 15 m^{-1}. For example, near 5000 K a hydroxyl concentration of 1.5×10^{15} cm^{-3} produces a peak signal-to-noise ratio of 16 with a peak absorption of 6.0 m^{-1}. Typical signal-to-noise ratios ranged between 10 and 100.

III. DATA ANALYSIS

A. Reaction mechanism and sensitivity analysis

The reaction mechanism for the H_2/O_2 system has been discussed by many authors. We use the mechanism of Miller and Bowman.[22] There are 8 reactive species in this scheme and 17 reactions. Of these only the reactions

$$H_2 + M \leftrightarrow 2H + M, \quad \text{(Rxn.1)}$$

$$H + O_2 \leftrightarrow OH + O, \quad \text{(Rxn.2)}$$

$$O + H_2 \leftrightarrow OH + H, \quad \text{(Rxn.4)}$$

$$OH + H_2 \leftrightarrow H_2O + H, \quad \text{(Rxn.6)}$$

play a significant role in creating and destroying hydroxyl at the high temperatures of our experiments.

Even though the hydrogen/oxygen system is the simplest chemical system in combustion, under the conditions used for our experiments, the system is complex enough to require numerical solutions of the coupled differential equations in order to describe its kinetic behavior. To evaluate the relative importance of different reactions in complex chemical systems, scientists have found it convenient to define sensitivity coefficients.[23] A sensitivity coefficient is simply the partial derivative of the concentration of a species of interest with respect to a specific rate coefficient. Reduced sensitivity coefficients, i.e., the sensitivity coefficient normalized by the concentration of the species of interest, are particularly useful for comparing sensitivities and designing experiments. Sensitivity coefficients may be conveniently calculated with the SENKIN[24] code. This code evaluates the concentration of the various species, the rate of change of the concentration, and the sensitivity coefficients for all species and reactions. An example of the reduced sensitivity coefficients for one of our high temperature experiments is shown in Fig. 2. Between 2 and 15 μs, the sensitivities to reactions (1) and (2) are about equal and together account for over 90% of the sensitivity to OH. At 15 μs all of the oxygen has been converted to OH. Therefore, beyond 15 μs only reaction (1), the rate of dissociation of H_2, is sensitive. Although reaction (6) appears to be sensitive at 2 μs, this sensitivity is too low to be important. To confirm this point we changed the rate of reaction (6) by more than a factor of 2 and noted that this

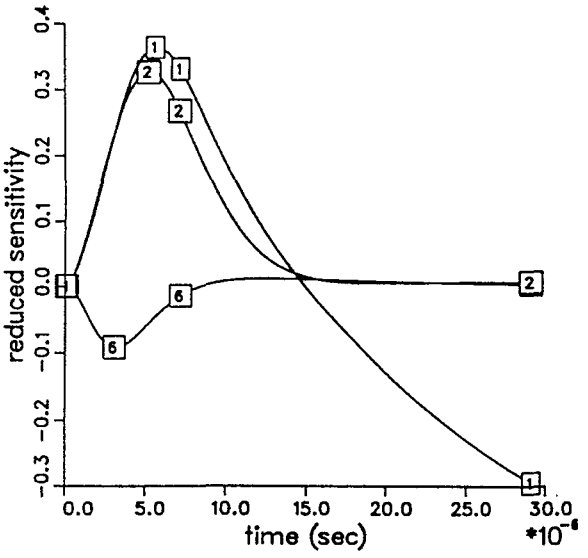

FIG. 2. Reduced sensitivity coefficients with respect to hydroxyl. Initial condition: $T = 5173$ K, $P = 96.1$ kPa, mole fractions: $H_2 = 1.6\times10^{-2}$, $O_2 = 1.5\times10^{-3}$, and Kr = 0.9825. The reaction numbers are defined in the text.

change had no effect on the resulting values for k_1 or k_2. Therefore, we may conclude that for fuel rich mixtures, $[H_2]/[O_2] \geqslant 10$, and high temperatures, $T \geqslant 3000$ K, we may use hydroxyl absorption profiles to simultaneously determine the rate of dissociation of H_2 and the rate of the $H + O_2$ reaction. We point out that at high temperatures our sensitivity analysis indicates that when hydroxyl is monitored there are no conditions where only the $H + O_2$ reaction dominates. For lower temperatures, $T \leqslant 3000$ K, the sensitivity analysis performed by Masten *et al.*,[16] Fig. 4(a) of Ref. 16, applies and the rate of the $H + O_2$ reaction accounts for over 90% of the sensitivity with respect to hydroxyl.

B. Least-squares analysis

Because the hydroxyl profile is sensitive to both reactions (1) and (2) at high temperatures, we must use a nonlinear least-squares technique[25] to determine the rate coefficients for these two reactions. There are many approaches for performing a least-squares analysis. We perform a chi-squared, χ^2, analysis and use the grid or quadratic algorithms described by Bevington[26] to determine the *best-fit* parameters. To determine the *confidence limits* (statistical uncertainties) of the *best-fit* parameters, we first look at the residuals. For the model to be acceptable, there must be no systematic deviation and the residuals must be uniformly distributed.[27] If these criteria are fulfilled, we weight each data point by $1/\sigma^2$, where σ is the root-mean-squared deviation of the best fit, invert the error matrix to obtain the correlation matrix, and determine its principle axis. We then change the length of the principle axis to find where χ^2 is increased by $\Delta\chi^2$. In general, we varied three or four parameters to determine the *best-fit* parameters. A multivariate distribution function[28] is used to determine the increase in χ^2 needed for a given confidence level. For example, when four variables are fit the increase in χ^2 is 4.72 for the 68% confidence level and 9.70 for the 95% confidence level.[29]

C. Kinetic model

To calculate the hydroxyl concentration we use the shock tube code developed by Mitchell and Kee[30] in conjunction with the new chemical kinetic interpreter, CHEMKIN-II version 2.4,[31] and the CHEMKIN thermochemical data base.[32] The advantages of using this set of codes are that they are readily available and the shock tube code uses the conservation laws of mass, momentum, and energy to describe the concentration, velocity, temperature, and pressure distributions behind the shock front. The rate coefficients for the reactions of the mechanism are entered into the kinetic interpreter as three parameters A_j, β_j, and E_j/k; $k_j(T) = A_j T^{\beta j} \exp[-E_j/kT]$. To obtain a *best fit* for a sensitive rate coefficient, we vary only the prefactor, A_j. After the least-squares analysis is complete, we determine the rate coefficient, $k_j(T)$, from the *best-fit* value of the prefactor, A_j^*, and the original values of β_j and E_j/k. Our original estimates for the parameters β_j and E_j/k were quite accurate. Therefore, we did not have to modify these parameters after the initial analysis and repeat the analysis. This approach accounted for changes in the rate coefficient as the temperature of the system changed. We then quote the rate coefficient at the temperature immediately behind the shock front, T_2. In the above shock tube code, the independent variable is time, not distance. To convert from "particle time" in the reference frame defined by the shock front to "laboratory distance," we use the equation[33]

$$t_{i+i} - t_i = \rho_i (x_{i+1} - x_i)/\rho_1 V_s, \tag{1}$$

where t_i is the particle time, ρ_i is the density at the position x_i behind the shock front, ρ_1 is the density in front of the shock front, and V_s is the speed of the shock front in the laboratory.

After the hydroxyl concentration has been calculated, we use the following equation to calculate the absorption profile, $\alpha(x_i)$, as a function of distance behind the shock front, x_i,

$$\alpha(x_i) = \frac{\pi e^2}{2mc\epsilon_0} f_{jk} g(\omega - \omega_0) P_j(x_i) n(x_i), \tag{2}$$

where the oscillator strength of the transition is f_{jk}, the normalized line shape function is $g(\omega - \omega_0)$, the probability that the initial level, $|j\rangle$, is occupied is $P_j(x_i)$, and the concentration of the hydroxyl is $n(x_i)$. The constant $\pi e^2/2mc\epsilon_0$ is 16.5×10^{-6} m^2 s^{-1}. The probability that the initial level, $|j\rangle$, is populated is calculated by standard expressions for the partition function, which uses spectroscopically determined parameters[34] to describe the energy level structure of the hydroxyl radical. To calculate properly the normalized line shape function, we need to know the line shape as a function of temperature and pressure. The group at Stanford has performed a series of beautiful experiments[35] to characterize the line shape of the ${}^RR_{11}(11/2)$ (0, 0) transition of the $A\,{}^2\Sigma^+ \leftarrow X\,{}^2\Pi_i$ system of hydroxyl. However, we have used a ${}^QQ$-branch transition, and therefore, we cannot use their

parameters. Instead, we have chosen to use the normalized Doppler profile and to treat the oscillator strength, f_{jk}, as a sensitive parameter to be determined by the least-squares analysis. We note that the oscillator strength does not alter a rate coefficient determined from a profile. Rate coefficients are determined by the shape of the profile, while the oscillator strength determines the amplitude of the profile. With this approach we can only determine the absolute concentration of hydroxyl to within a factor of two, but this is unimportant since all reactions have only one set of products.

D. Instrumental uncertainties

Instrumental uncertainties in chemical kinetic experiments are often larger than the statistical uncertainties. Therefore, we must realistically assess the source and magnitude of the instrumental uncertainties. For the flash-absorption technique the largest instrumental uncertainty results from our inability to control the profile of the light pulse from shot to shot. Simply stated, shot-to-shot changes of the profile of the light beam will introduce changes in the absorption profile which lead to changes in the calculated rate coefficients. To estimate the uncertainty introduced by these shot-to-shot changes we measured profiles for a series of shocks in pure argon. From these studies, we conclude that a measured absorption profile may deviate from the "true" absorption profile as a linear function of the distance behind the shock front. The further behind the shock front, the larger the deviation. We have taken several profiles at different temperatures and modified them to account for this instrumental uncertainty, and then re-evaluated the rate coefficients. From this, we conclude that the rate coefficient for hydrogen dissociation has an instrumental uncertainty of approximately 25%, while the rate coefficient for $H + O_2 \rightarrow OH + O$ is uncertain by approximately 10%. For hydrogen dissociation the instrumental uncertainty is the dominant uncertainty. For the titled reaction, at low temperatures the instrumental uncertainty also dominates; at the highest temperatures, the instrumental and statistical uncertainties are comparable. Therefore, at high temperatures, we combined these two uncertainties in quadrature. The uncertainties quoted in the tables represent an estimate of the standard deviation as if we had made a large number of independent measurements at a single temperature.

In addition to instrumental uncertainties introduced by the absorption profiles, we also estimate the uncertainties associated with the calculation of the temperature behind the incident shock front. The uncertainty in this calculation comes from the uncertainty in the measurement of the initial temperature of the gas in the shock tube, T_1, and the velocity of the shock front, V_s. These uncertainties are calculated and combined to give a conservative estimate of the uncertainty in the calculation of the Mach number, M_1. We express the fractional uncertainty in the Mach number as

$$\left(\frac{\delta M_1}{M_1}\right)=\left(\frac{\delta V_S}{V_S}\right)+\frac{1}{2}\left(\frac{\delta T_1}{T_1}\right), \tag{3}$$

where δV_s is the 2σ uncertainty of the speed of the shock front and δT_1 is the uncertainty of the initial temperature of the gas within the shock tube, 0.5 K. The fractional uncertainty in the initial temperature behind the shock front is then calculated by differentiating the Rankine–Hugoniot equations.[36] Because we are probing only a short distance behind the shock front, less than 20 mm, boundary layer corrections[37] are not necessary.

IV. RESULTS

We performed measurements with four different mixtures, one made with argon and the other three with krypton carrier gases. The results divide themselves into two distinct groups: a high-temperature group, $T > 3000$ K, and a low-temperature group, $T < 3000$ K. Above 3000 K the rate of dissociation of H_2, k_1, may be experimentally determined along with the rate for $H + O_2 \rightarrow OH + O$, k_2. Below 3000 K, we may only determine the rate of the latter reaction.

It is convenient to begin this discussion with the highest temperature results. Figure 3 shows an absorption profile obtained at 5173 K. After the diffraction spikes, which we use to determine the location of the physical origin of the shock front, and a short incubation period (to be discussed below) the hydroxyl concentration rises rapidly, peaks 5 mm behind the shock front (this corresponds to 10 μs in the particle frame), and then slowly decays. The solid line represents the best fit when we varied three parameters: two preexponential rate parameters, A_1 and A_2, and the oscillator strength, f. Clearly, at early times, the kinetic model does not reproduce the measured absorption profile. This is shown in more detail in Fig. 4(a) where we plot the residuals from the χ^2 analysis. To obtain agreement between the kinetic model and the observations we must assume the start of the absorption by hydroxyl is shifted some distance from the physical origin defined by the shock front. We treat this

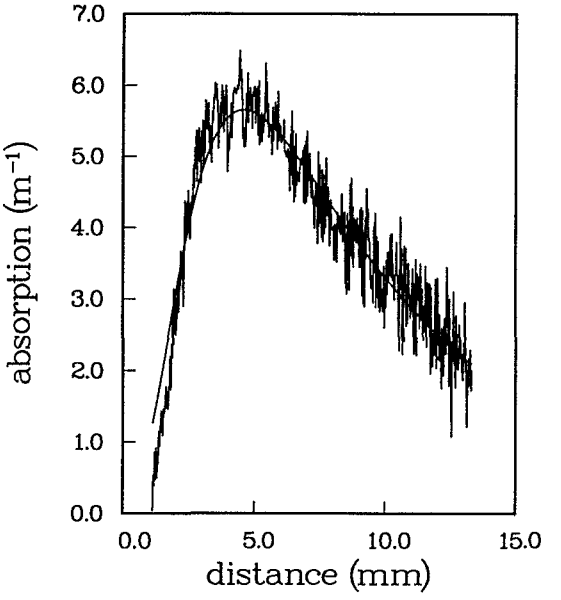

FIG. 3. Absorption profile of hydroxyl. Conditions are the same as in Fig. 2. The solid line represents the best fit when only A_1, A_2, and f are varied. See the text for discussion.

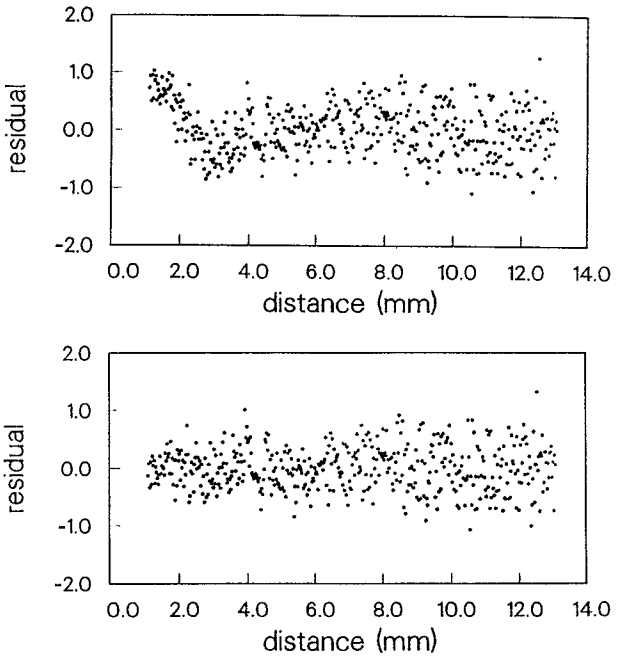

FIG. 4. Residuals from the χ^2 fit of the profile shown in Fig. 3. Upper part, $x_c = 0.0$, lower part $x_c = 0.783$ mm.

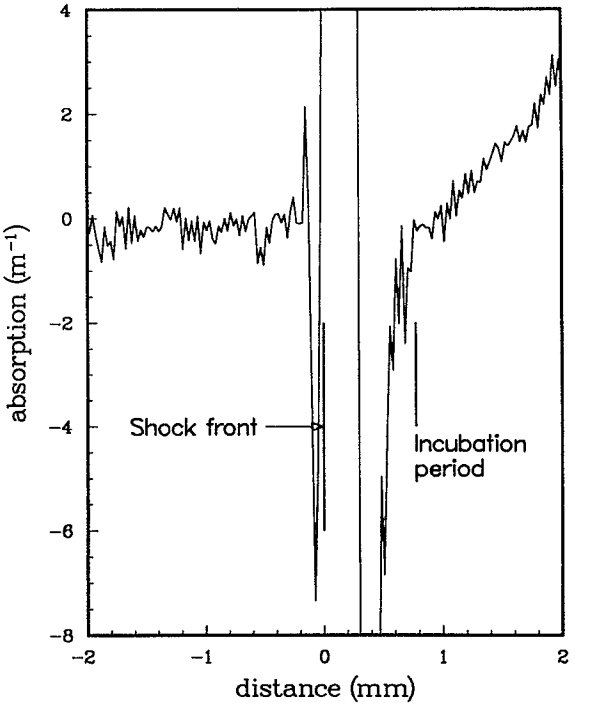

FIG. 5. Detail of the absorption profile near the shock front of Fig. 3. The shock front is located at the origin of the x axis and the vertical line at 0.783 mm denotes the end of the incubation period and the start of the absorption by the hydroxyl radical. See the text for discussion.

shift, x_c, as a sensitive parameter and determine its magnitude in the χ^2 analysis. The improvement is shown in Fig. 4(b), where we have varied four parameters: A_1, A_2, f, and x_c.

The details of the difference between the physical origin and the start of absorption are shown in Fig. 5. Previously, we discussed[21] the use of the 1D Huygen's diffraction integral[38] in the Fresnel approximation to calculate the diffracted wave function incident on the array detector in terms of the wave function diffracted by the curvature of the shock front. From this analysis we determine the location of the shock front (shown as the origin in Fig. 5) and estimate the curvature of the shock front to be less than 0.2 mm. In front of the shock wave, negative distances in the figure, the absorption profile is flat. The initial spike, which rises to 2.0 and then drops to -7.5, is due to diffraction by the surface of the shock front. The physical origin of the shock front is determined by the onset of a large absorption spike. This spike is caused by the curved surface of the shock front refracting the light. This refracted light appears as an intense negative spike directly behind the positive spike. The smaller spikes which follow the intense spikes are due to diffraction. Shortly after the negative spike, the absorption returns to zero and absorption by the hydroxyl radical slowly appears. The vertical line at 0.8 mm locates the fitted start of the absorption profile. Profiles similar to Fig. 5 are obtained at all high temperatures.

By including the shift in the absorption profile, all of the calculated profiles fit the measured profiles very well when only four parameters (A_1, A_2, f, and x_c) are varied. The results for the high-temperature measurements are given in Table I. The rate coefficients for the dissociation of H_2 are shown in Fig. 6. The solid line represents a least-squares fit of our results to give

$$k_1(T) = (8.86 \pm 0.88) \times 10^{-10} \times \exp[-48321/T(\mathrm{K})]\,\mathrm{cm^3\,s^{-1}}, \quad (4)$$

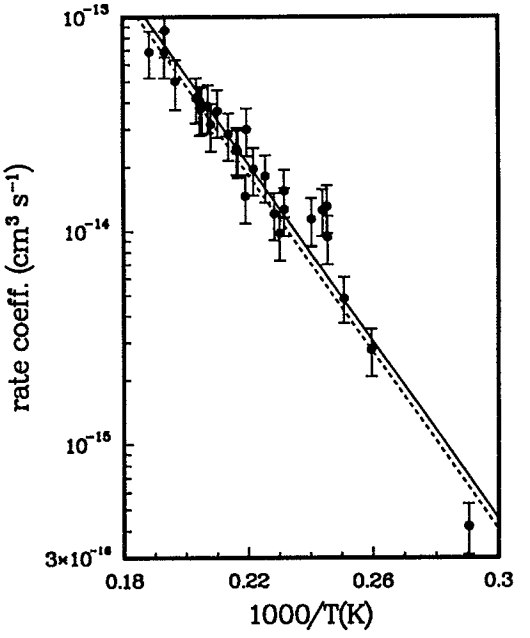

FIG. 6. Rate coefficient for the dissociation of H_2 in krypton. The error bars represent $\pm\sigma$. The solid line represents the least-squares fit of the data, Eq. (4). The dashed line represents previous measurements in Kr, Ref. 59.

TABLE I. High-temperature rate data for the $H_2 + M \rightarrow 2H + M$ and $H + O_2 \rightarrow OH + O$ reactions.

P_1 (kPa)	M_1[a]	P_2 (kPa)	T_2[a] (K)	N[b]	rmsd[c] (m^{-1})	$H_2 + M$[d] (10^{-15} $cm^3 s^{-1}$)	$H + O_2$[d] (10^{-12} $cm^3 s^{-1}$)	x_c[d] (mm)
	$X_{H2} = 4.380\times10^{-2}$, $X_{O2} = 4.100\times10^{-3}$, $X_{Kr} = 0.952\ 100$							
3.340	6.003	149.58	3446	432	0.302	0.42	21.1	0.27
	0.016		24			0.11	2.4	0.12
2.005	6.375	101.41	3853	541	0.207	2.78	24.8	0.829
	0.017		27			0.70	2.5	0.018
2.402	6.496	126.20	3986	616	0.214	4.9	27.9	0.824
	0.018		28			1.2	3.5	0.082
2.139	6.573	115.05	4075	551	0.239	13.1	25.2	0.91
	0.018		29			3.3	9.1	0.24
1.936	6.647	106.50	4160	557	0.372	11.4	24.8	0.907
	0.018		30			2.9	3.7	0.088
1.747	6.781	100.05	4316	555	0.294	15.5	24.8	0.736
	0.019		32			3.9	3.8	0.092
1.752	6.831	101.85	4376	545	0.286	12.1	29.9	0.753
	0.019		32			3.0	4.5	0.089
1.739	6.883	102.62	4432	556	0.192	18.1	29.4	0.795
	0.019		32			4.5	3.3	0.034
1.736	6.938	104.13	4509	559	0.300	19.6	33.9	0.715
	0.019		32			4.9	3.9	0.036
	$X_{H2} = 2.185\times10^{-2}$, $X_{O2} = 2.047\times10^{-3}$, $X_{Kr} = 0.976\ 103$							
2.538	6.507	133.75	4072	547	0.381	9.4	25.5	1.187
	0.017		28			2.4	3.6	0.099
2.156	6.712	120.91	4315	557	0.329	12.7	29.6	0.995
	0.018		30			3.2	3.4	0.052
1.963	6.908	116.64	4554	546	0.332	29.9	32.3	1.056
	0.019		33			7.5	5.3	0.083
1.679	6.912	99.89	4561	554	0.477	14.6	38.8	0.81
	0.019		33			3.7	5.8	0.11
1.908	6.959	115.09	4612	555	0.288	23.7	36.4	0.793
	0.019		33			5.9	5.2	0.069
1.869	6.962	112.86	4622	545	0.326	24.4	37.3	0.888
	0.019		33			6.1	5.5	0.076
1.777	7.012	108.87	4677	471	0.400	28.5	36.7	0.880
	0.020		35			7.1	5.7	0.080
1.788	7.072	111.40	4756	551	0.286	36.5	28.7	0.828
	0.020		35			9.1	4.5	0.084
1.720	7.105	108.18	4804	555	0.503	31.5	33.5	0.71
	0.020		35			7.9	6.1	0.11
	$X_{H2} = 1.607\times10^{-2}$, $X_{O2} = 1.505\times10^{-3}$, $X_{Kr} = 0.982\ 425$							
2.408	6.514	127.71	4098	539	0.335	12.6	22.3	1.361
	0.017		28			3.1	2.3	0.022
2.134	6.720	120.29	4344	559	0.426	9.8	31.5	0.86
	0.018		31			2.5	4.6	0.13
1.639	7.100	102.92	4824	545	0.277	38.4	28.6	0.878
	0.020		35			9.6	3.9	0.083
1.565	7.128	98.01	4871	460	0.328	37.8	42.5	0.759
	0.020		36			9.5	6.3	0.085
1.689	7.151	107.61	4888	559	0.171	37.5	35.2	0.739
	0.020		36			9.4	4.0	0.039
1.471	7.153	93.74	4914	559	0.466	42.	28.8	0.79
	0.020		36			10.	5.0	0.14
1.469	7.303	97.66	5082	543	0.479	50.	43.	0.83
	0.021		36			13.	10.	0.16
1.376	7.371	93.16	5169	338	0.526	87.	26.4	1.05
	0.021		38			22.	4.5	0.12
1.421	7.334	94.88	5173	457	0.376	69.	37.8	0.783
	0.021		38			17.	5.7	0.085
1.336	7.472	92.97	5305	396	0.292	69.	28.2	0.549
	0.020		37			17.	3.6	0.074

[a] The numbers below the Mach number and temperature represent a confidence limit of 95.4%.
[b] The number of points used to fit the profile.
[c] The root-mean-squared deviation of the *best-fit* profile.
[d] The numbers below the parameters are the 1-σ uncertainties.

where the uncertainty is at the 95% confidence level. The r.m.s.d. for $\ln[k_1(T)]$ is 0.288. If we vary both the prefactor and the activation energy, the r.m.s.d. for $\ln[k_1(T)]$ decreases very slightly to 0.281, but the uncertainty in each parameter increases significantly. Therefore, to retain the same activation energy as in previous measurements, we use the above equation. We note that the observed deviation of 28% is consistent with our assigned instrumental uncertainty of 25%.

The results for the rate coefficient for the titled reaction at high temperatures are also summarized in Table I. At high temperatures, the rate of production of hydroxyl is very rapid. Therefore, the *best-fit* parameters for the rate coefficient and the shift in the origin are correlated. This correlation produces a significant statistical uncertainty in the evaluation of the rate coefficient at high temperatures. This is demonstrated in Fig. 7, where we show χ^2 contours[39] for $\Delta\chi^2 = 4.72$ and 9.70. Clearly, as the shift in the origin increases the *best fit* to the rate coefficient also increases to maintain a minimum χ^2. Because of this correlation, at high temperatures the statistical and instrumental uncertainties in k_2 are comparable. The coefficients k_1 and k_2 are not correlated because k_1 is determined by the entire absorption profile while k_2 is only determined by the early part of the profile.

In the low-temperature region, the absorption profiles show the characteristic ignition delay time, followed by a relatively rapid rise in hydroxyl concentration which levels out at the equilibrium value. A profile from the low-temperature region is shown in Fig. 8. To extract rate coefficients from the low-temperature measurements we used expression (4) for k_1 in krypton and Miller and Bowman's expression[22] for k_1 in the argon system. In all cases, k_1 was held fixed. Unlike the situation above 3000 K, where the dissociation of H_2 is initiating the chain-branching reactions, below 3000 K the initiation reaction cannot be identified. As suggested by Masten *et al.*,[16] we varied the rate of the reaction $H + HO_2 \leftrightarrow H_2 + O_2$ to shift some profiles with respect to the origin. The resulting values for this rate coefficient did not show any systematic trend. Since the shift of the origin of the absorption simply moves the profile with respect to the physical origin of the shock front, we fixed the rate coefficient of the above reaction and varied the shift parameter, x_c, for the results reported here. The parameters x_c and k_2 are correlated, just as discussed above, but now the statistical uncertainty in k_2 is insignificant. For example, even with the correlation, at 2481 K the statistical uncertainty in k_2 is less than 0.5% while the instrumental uncertainty is 10%. Our results for the low-temperature region are summarized in Table II.

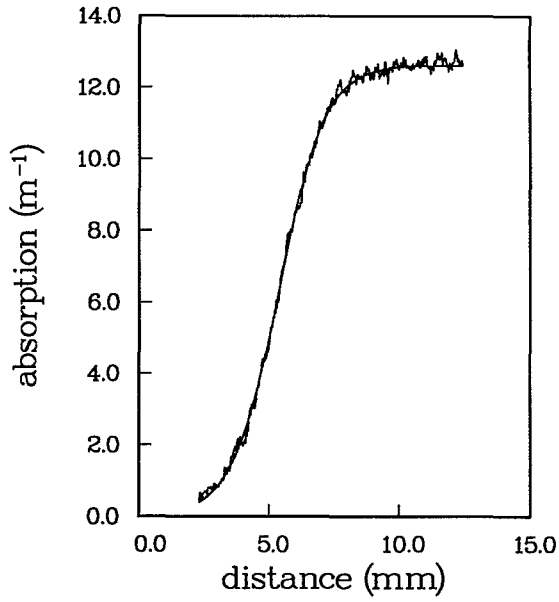

FIG. 8. Absorption profile obtained at a temperature of 2481 K. The solid line represent the best fit when A_2, f, and x_c are varied.

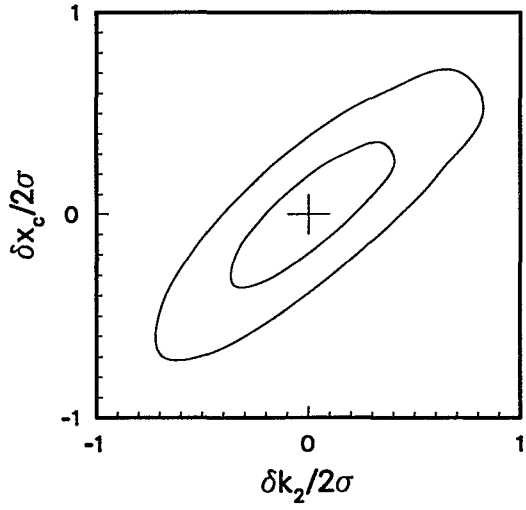

FIG. 7. Contours of constant $\Delta\chi^2$ for the profile of Fig. 3. k_1 is held fixed at the *best-fit* value. The $\delta k_2/2\sigma$ and $\delta x_c/2\sigma$ axis are fractions of the 2-σ uncertainty in k_2 and x_c, respectively.

All of our results for the rate coefficient of the titled reaction are shown in Fig. 9. A least-squares analysis of our results gives

$$k_2(T) = (1.55 \pm 0.25) \times 10^{-10} \times \exp[-7270 \pm 520/T(\mathrm{K})]\,\mathrm{cm^3\,s^{-1}}, \quad (5)$$

where the uncertainties are at the 95% confidence level. The r.m.s.d. for $\ln[k_2(T)]$ is 0.123. The value for the reduced χ^2, χ^2 divided by the number of degrees of freedom, is 1.03. Therefore, our assignments of the instrumental and statistical uncertainties are consistent with the deviations of the points. For comparison, in Fig. 9, we have included the higher-temperature data from Masten *et al.*,[16] five points from Shin and Michael,[19] the analytic expressions of Yuan *et al.*,[17] Frank and Just,[10] and the latest expression of Fujii *et al.*[15]

TABLE II. Low-temperature rate data for the H + O$_2$ → OH + O reaction.

P_1 (kPa)	M_1[a]	P_2 (kPa)	T_2[a] (K)	N[b]	rmsd[c] (m^{-1})	H + O$_2$[d] (10^{-12} cm^3 s^{-1})
	$X_{H2} = 3.978\times10^{-2}$, $X_{O2} = 4.213\times10^{-3}$, $X_{Ar} = 0.956\,007$					
6.514	4.484	161.77	2050	343	0.341	4.21
	0.012		13			0.42
5.672	4.575	146.72	2124	855	0.416	4.51
	0.012		14			0.46
4.668	4.780	131.96	2294	571	0.457	6.87
	0.013		15			0.71
3.332	5.120	108.21	2592	649	0.234	9.83
	0.015		18			0.99
2.536	5.327	89.26	2791	638	0.461	12.3
	0.016		21			1.2
2.400	5.365	85.66	2827	637	0.305	11.2
	0.016		22			1.1
2.008	5.490	75.099	2946	657	0.244	14.6
	0.017		23			1.5
	$X_{H2} = 4.380\times10^{-2}$, $X_{O2} = 4.100\times10^{-3}$, $X_{Kr} = 0.952\,100$					
8.123	4.651	217.25	2179	633	0.252	5.39
	0.010		12			0.54
6.690	5.003	207.34	2481	403	0.153	7.03
	0.011		14			0.70
5.022	5.370	179.66	2815	235	0.222	12.9
	0.013		18			1.3
5.069	5.460	187.46	2899	327	0.236	14.4
	0.013		19			1.5

[a] The numbers below the Mach number and temperature represent a confidence limit of 95.4%.
[b] The number of points used to fit the profile.
[c] The root-mean-squared deviation of the *best-fit* profile.
[d] The numbers below the parameters are the 1-σ uncertainties.

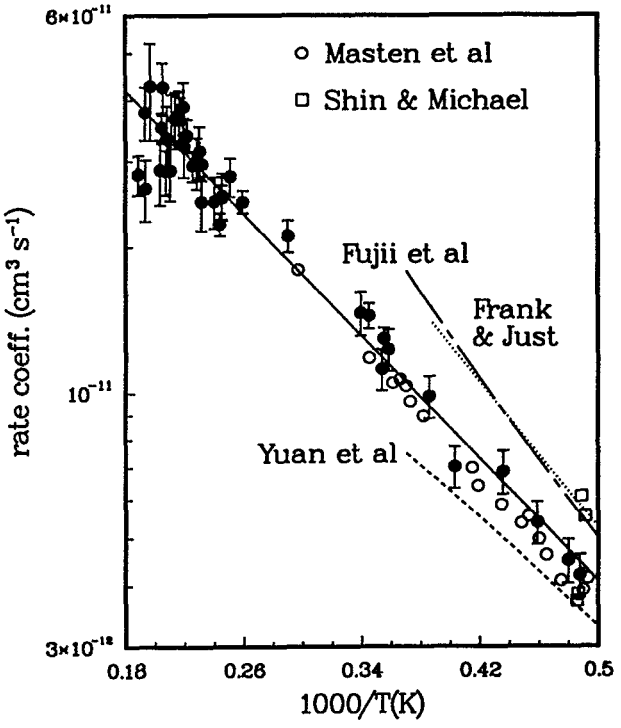

FIG. 9. Rate coefficient for the H + O$_2$ reaction. The error bars represent ± σ. The solid line represents the least-squares fit of the data, Eq. (5). For references to the other experimental works see the text.

V. DISCUSSION AND CONCLUSIONS

A. Shift of the absorption profile

The observed shift of the start of the absorption profile may be caused by two effects. First, the curved shock front convolutes all measurements at a given distance. This effect was discussed in our previous paper[21] and, at most, can introduce a shift that is less than the curvature of the shock front, ~0.2 mm. The observed shifts are approximately five times larger. Another physical effect which produces an apparent shift in a reacting chemical system is the incubation time.[40] Naïvely, the incubation time is the time between the instantaneous heating of the buffer gas and the time for the reaction to commence. Generally, this time is comparable to the vibrational relaxation time of the molecules and depends upon the measurement scheme. Incubation times have been observed in many systems: the dissociation of diatomic molecules,[41] the dissociation of nitrous oxide,[42] and the thermal isomerization of cyclopropane.[43] Since dissociation of H$_2$ initiates the chain-branching reactions above 3000 K, the incubation time should be related to the rate of relaxation of molecular hydrogen. The most useful approach for calculating incubation times is an analytic approximation developed by Penner and Forst[44] and extended to include vibrational–rotational energy transfer by Forst.[45] In this approach, the simple exponential model of transition probabilities[46] is used and analytic expressions are derived which use mea-

sured relaxation times and the dissociation energy to calculate the energy transferred per collision and the effective threshold for dissociation. These parameters are then used to solve for the dissociative rate constant and the incubation time. Dove and Titelbaum[47] have measured the relaxation rate of H_2 in the inert gases. We have used their relaxation times and Forst's theory to calculate the incubation time for all of our measurements above 3000 K. Although our results are scattered significantly, they fall between the measured relaxation times and the calculated incubation times. Therefore, we may conclude that the observed shift in the absorption profile is simply the time required for the system to initiate the chain-branching reactions and is due to the finite rate of relaxation of molecular hydrogen.

B. Relaxation processes

As demonstrated above, as shock tube experiments are performed at higher and higher temperatures, the rate of reaction of the chemical system approaches the rate of relaxation of the molecular species. Therefore, to insure that our measurements reflect a rate coefficient at equilibrium, we must evaluate all relaxation processes.

First, we address the vibrational relaxation of O_2. The rate of translational-to-vibrational energy transfer between Ar and O_2 from 1200 to 7000 K has been measured by Camac.[48] White and Millikan[49] have measured the rate of relaxation of O_2 by H_2 between 400 and 2000 K; H_2 is a very efficient relaxer of O_2. Millikan and White[50] have derived an empirical equation to describe the relaxation of simple systems. For the relaxation of molecular oxygen their formula reduces to

$$\ln_e(P\tau) = D\mu^{1/2}(T^{-1/3} - 0.015\mu^{1/4}) - 18.42, \quad (6)$$

where the pressure of the gas in atmospheres is P, the relaxation time in seconds is τ, the reduced mass of the collision partners is μ, the temperature in Kelvins is T, and the constant, D, is 39.25 or 31.05 $K^{1/3}$ for O_2–Ar or O_2–H_2 collisions, respectively. More recently, Subba Rao and Skinner[51] have measured the rate of relaxation of O_2 in the presence of both Ar and H_2 from 860 to 1290 K. Their results confirm the previous measurements and are consistent with the linear-mixture rule. We have used the above equation to calculate the relaxation times for O_2–Kr, O_2–Ar, and O_2–H_2 collisions and applied the linear-mixture rule to calculate the relaxation time for the gas mixture. For our experimental conditions near 5000 K the vibrational relaxation time for O_2 is 0.95 μs. This may be compared to an incubation time of 2.0 μs and the time required to produce 10% of the peak hydroxyl concentration, 2.8 μs. Near 2000 K, the relaxation time of O_2 is 2.0 μs; the time required to produce 10% of the peak hydroxyl concentration is 35 μs. Therefore, near 2000 K the vibrational temperature of O_2 is within 1% of the bath temperature well before the hydroxyl radical is observed.

At our highest temperatures, the rate of vibrational relaxation of O_2 is faster than, but comparable to, the rate of the chemical reaction. Therefore, one must ask, "Does this rate of relaxation affect the measured rate coefficient?" To address this question we use the results of Montroll and Shuler[52] to calculate the vibrational distribution of O_2 during the relaxation process. They have shown that a system of harmonic oscillators which relax via $\Delta v = \pm 1$ transitions only and have an initial Boltzmann distribution will relax to a final Boltzmann distribution via a continuous sequence of Boltzmann distributions. Therefore, throughout the entire relaxation process we may describe the vibrational distribution of the O_2 molecules by a temperature. In particular, for experiments near 5000 K the vibrational temperature of the O_2 molecules at the end of the incubation period is 4430 K and when 10% of the hydroxyl has been formed this temperature is 4750 K. For the level-dependent rate coefficients we use Miller's[8] calculated rate coefficients. At 5000 K, the ratios of the rate coefficients for O_2 in the lower vibrational levels to the rate coefficient for $v = 0$ are 1.3, 1.9, 2.3, and 2.5 for $v = 1$, 2, 3, and 4, respectively. If the O_2 vibrational temperature is reduced by 10% to 4500 K, the overall rate coefficient is reduced by only 0.8%.

From these calculations we may conclude the following. At low temperatures the vibrational temperature of O_2 is in equilibrium with the bath gases well before we observe the formation of hydroxyl. At the highest temperatures the vibrational temperature of O_2 is within approximately 10% of the equilibrium temperature at the end of the incubation period. Therefore, the measured rate coefficient should reflect the overall bimolecular rate coefficient at the temperature of the buffer gas. However, the actual dynamics of the relaxation process could be more complicated and the level-dependent rate coefficients could vary more strongly. Whether O_2 is indeed in equilibrium, as we have calculated, can be determined by measuring the relaxation rates of specific vibrational levels of O_2 at high temperatures. Our apparatus has the potential to carry out such measurements and, presently, we are designing these experiments.

Finally, we consider the rotational and vibrational relaxation of the product radical, hydroxyl. Since we are employing a detection scheme which monitors the population in a specific rovibrational level, we can only extract rate coefficients if the radical is in thermodynamic equilibrium with the buffer gas. The cross sections for rotational energy transfer[53] have been measured for the f_1 (2) level in $v = 2$ with He as a collision partner. We assume they are comparable for $v = 0$ and 1 and extrapolate to our conditions; we obtain a rotational energy transfer rate between 1 and 2×10^8 s^{-1}. Therefore, for our experiments, the rotational temperature is equal to the bath temperature. Rate coefficients for vibrational energy transfer from OH ($X\,^2\Pi_i$, $v = 2$ and 1) have been measured for collisions with molecular hydrogen and water,[54] molecular oxygen,[55] and atomic hydrogen[56] and oxygen.[57] Atomic hydrogen and oxygen are the most efficient collision partners. The energy transfer rate from $v = 2$ to $v = 1$ at 3000 K and a hydroxyl concentration equal to 10% of its peak concentration is 3.8×10^6 s^{-1} ($\tau_{relax} = 263$ ns). At our highest temperature, 5300 K, the analogous rate is 1.8×10^6 s^{-1} ($\tau_{relax} = 556$ ns). As the reactions proceed, the relaxation times will decrease by a factor of 10. These relaxation rates are comparable to the rate of the chemical reactions. Therefore, if hydroxyl were created in a nonstatistical vibrational distribution we would have to account for the rate of vibrational relaxation. Kleinermanns and

Schinke[58] have performed classical trajectory calculations of total and state-to-state cross sections. Below $E_{c.m.} = 1.2$ eV (14,100 K) they find that OH is produced with both rotational and vibrational distributions in thermal equilibrium. Therefore, we may assume that measurements of the temporal behavior of any rovibrational level will reflect the temporal behavior of the concentration of hydroxyl.

C. H_2 dissociation rate

There have been many experimental studies of the dissociation rate of H_2. They have been reviewed most recently by Cohen and Westberg.[5] Almost all of the studies have been performed in argon. The only study in krypton was performed by Rink.[59] If we use the equilibrium constant to convert Rink's published recombination rate into a low-pressure dissociation rate, we obtain

$$k_1(T) = 2.11\times10^{-5}T^{-1.1}\exp[-52530/T(\mathrm{K})]\ \mathrm{cm^3\,s^{-1}}. \quad (7)$$

This agrees to within 11% with our results and is shown as the dashed line in Fig. 6. From this comparison, we conclude that our results are in agreement with the only previous measurement and that further work is needed on the rate of dissociation of H_2 in different buffer gases.

D. $H+O_2 \rightarrow OH+O$ rate

Of the recent measurements of the rate of this reaction, the work most analogous to our study is that of Masten *et al.*[16] We both detected the hydroxyl radical, our initial concentrations are approximately the same, the $[H_2]$-to-$[O_2]$ ratios are identical, and we used the same reaction mechanism to evaluate our results. Although we used a different detection technique, our results overlap with those of Masten *et al.* over the common temperature range, 2050 to 3300 K. At the lowest common temperature, where the disagreement is the largest, the two results differ by only 8.3%. This is within the experimental uncertainty of both measurement sets.

Our lowest temperature measurement just coincides with the highest temperature results of the new measurements by Shin and Michael.[19] They used a laser to photolyze H_2O or NH_3 to produce hydrogen atoms and then detected the decay of the hydrogen atoms with atomic resonance absorption spectrophotometry. At 2050 K, their Arrhenius expression falls 11% below our measurements, which is well within the standard deviation of Shin and Michael's results. The initial mole fractions of oxygen used by Shin and Michael were comparable to our initial concentrations and the ratios of the concentrations of the hydrogen precursor to oxygen were all <1.0. In experiments which measure hydroxyl in rich mixtures all of the oxygen is consumed, whereas in the laser photolysis experiments very little oxygen is consumed. In spite of these differences, the measurements agree to within experimental uncertainty. Since the photolysis experiments do not depend upon relaxation of the hydroxyl radical for an evaluation of the rate coefficient, this agreement supports our contention that measurements of $v=0$ hydroxyl reflect the equilibrium OH concentration, and therefore, the rate of the reaction.

Other recent measurements of hydroxyl do not agree with our results. The earlier work from Gardiner and coworkers used rich mixtures, $[H_2]$-to-$[O_2]$ ratios of 10, to measure the rate of formation of hydroxyl over the temperature range 1900 to 2650 K. In their later work, they combined these results with additional data obtained with O-atom absorption measurements and previously obtained low-temperature measurements to derive the positive non-Arrhenius behavior given by[15]

$$k_2(T) = 16.6\times10^{-18}T^{2.0}\exp[-5172/T(\mathrm{K})]\ \mathrm{cm^3\,s^{-1}} \quad (8)$$

over the temperature range 1100 to 2700 K. At 2700 K, their result is 70% higher than our measured value. This corresponds to seven of our standard deviations. Frenklach's group used very lean to moderately rich mixtures, $[H_2]$-to-$[O_2]$ ratios from 0.1 to 4.0, to study the reaction between 1050 and 2700 K. They recommend[17]

$$k_2(T) = 2.64\times10^{-7}T^{-0.927}\exp[-8493/T(\mathrm{K})]\ \mathrm{cm^3\,s^{-1}} \quad (9)$$

with a 1-σ standard deviation in $\log_{10}[k_2(T)] = 0.05$. At 2700 K, their result is 30% lower than our measured value. This corresponds to three of our standard deviations. The reasons for these disagreements are not clear.

To extract an analytic expression for the rate coefficient over a relatively large temperature range, we note that Pirraglia *et al.*[18] used the flash-photolysis technique and obtained

$$k_2(T) = (2.79\pm0.32)\times10^{-10} \times\exp[-(8119\pm139)/T(\mathrm{K})]\mathrm{cm^3\,s^{-1}} \quad (10)$$

for the temperature range 962–1705 K. The uncertainties are at the 68% confidence level. Because our results, the results of Masten *et al.*,[16] the new results of Shin and Michael,[19] and the results of Pirraglia *et al.*[18] agree to within their respective experimental errors, they form a complete and overlapping set of data. We combine these four data sets to produce a single data set from 960 to 5300 K. The density of data points is much larger in the data of Shin and Michael and Pirraglia *et al.* than in Masten *et al.*'s and our data, therefore, we use Shin and Michael's and Pirraglia *et al.*'s analytic expressions to calculate rate coefficients at equal increments of $1000/T(\mathrm{K})$. From this, we obtain 158 data points which are equally distributed over the entire range of reciprocal temperature. We weight each data set by the inverse of the square of the standard deviation of the respective fits. A nonlinear least-squares analysis gives the expression

$$k_2(T) = 4.06\times10^{-10}T^{-0.11\pm0.29} \times\exp[-(7685\pm595)/T(\mathrm{K})]\mathrm{cm^3\,s^{-1}}. \quad (11)$$

The 2σ uncertainty in $\ln[A] = 0.12$. The uncertainty in the parameters β and E/k are at the 2σ, or 95% confidence level. These apparently large uncertainties arise because the parameters are highly correlated. The r.m.s.d. for

$\ln[k_2(T)]$ was 0.092. Since the β coefficient may be equal to zero, we refit the data without the temperature dependent prefactor. This gave the Arrhenius expression

$$k_2(T) = (1.62 \pm 0.12) \times 10^{-10} \times \exp[-(7474 \pm 122)/T(\mathrm{K})]\,\mathrm{cm^3\,s^{-1}}. \quad (12)$$

Again, the uncertainties are at the 95% confidence level. The r.m.s.d. for $\ln[k_2(T)]$ was 0.093. Since the data of Shin and Michael and Pirraglia *et al.* are basically over the same temperature range, we removed first one and then the other data set and refit the remaining three data sets. Although the parameters obtained from each fit are slightly different, the non-Arrhenius behavior remains statistically insignificant and consistent with $\beta = 0$. Therefore, *we conclude that the rate coefficient of the* $H+O_2 \rightarrow OH+O$ *reaction follows an Arrhenius expression over the temperature range 960 to 5300 K.* We compare our recommended expression for the rate coefficient, Eq. (12), with the recommendation of Cohen and Westberg. At 1000 K, the two expressions differ by only 4.9%. This is well within their suggested uncertainty and our calculated standard deviation.

We now compare our recommendation to calculations of the rate coefficient. Transition-state theory has been superseded by quasiclassical trajectory and quantum scattering calculations for bimolecular exchange reactions of triatomic systems. Accurate potential-energy surfaces are now available for triatomic systems and trajectory and scattering calculations provide more detailed information about the dynamic aspects of the reaction. A schematic representation of the reaction path for the hydroperoxyl radical is shown in Fig. 10. Spectroscopic measurements provide important parameters for the potential-energy surface at specific points.

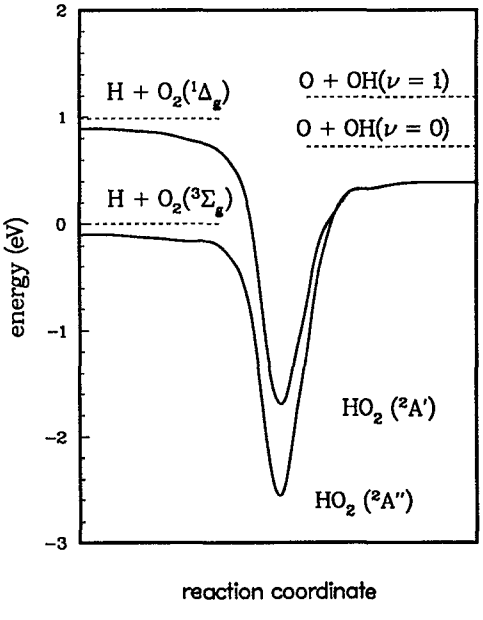

FIG. 10. Potential-energy profiles. Dashed lines represent real energy levels measured spectroscopically.

From the dissociation energies[60] of O_2 and OH, we can write $H(^2S) + O_2(^3\Sigma_g^-,\ v=0) + 724$ meV $\rightarrow OH(^2\Pi_i,\ v=0) + O(^3P)$. In addition, in the entrance channel the $O_2(^1\Delta_g,\ v=0)$ level is only 982 meV above the ground level. From near infrared absorption[61] and emission[62] spectra, the splitting between the ground and first excited electronic levels of the intermediate hydroperoxyl radical, HO_2, is 880 meV. From the bond dissociation energy of the hydroperoxyl radical,[63] the ground level of the HO_2 radical is 2095 ± 52 meV below $H + O_2$.

The first realistic potential-energy surface extending into the practical interaction range was calculated by Melius and Blint.[9] Although this surface has been used for many dynamic calculations, it has four deficiencies: (i) it shows a barrier (~ 100 meV) in the entrance channel along the minimum energy path, (ii) it does not give the correct well depth for the hydroperoxyl radical, (iii) it does not correctly describe the saddle point of the H-atom exchange region, and (iv) the O + OH part of the surface was not characterized. Langhoff and Jaffe[64] suggested there is no barrier in the $H(^2S) + O_2(^3\Sigma_g^-)$ channel and possibly a small barrier in the $H(^2S) + O_2(^1\Delta_g)$ channel. Also, they showed that the $H(^2S) + O_2(^3\Sigma_g^-)$ surface correlates with the $^2A''$ ground surface of HO_2 while the $H(^2S) + O_2(^1\Delta_g)$ surface correlates with the excited $^2A'$ surface. Because most studies have been performed at low temperatures, the $H(^2S) + O_2(^1\Delta_g)$ channel and, therefore, the $^2A'$ surface have been neglected. Dunning *et al.*[65] performed large scale polarization configuration interaction (POL-CI) calculations on the potential surface for hydrogen atom addition and found the barrier to be less than 17 meV and possibly zero. While the above studies provide a fairly complete description of the forward channel, $H + O_2$, most recent work has concentrated on the reverse channel, OH + O. *Ab initio* calculations on the form of the OH + O interaction were provided by Walch *et al.*[66] Their study confirmed that no barrier exists for the addition of an H atom to O_2 and a small barrier (20 meV) exists for the recombination of OH and O. Walch and Rohlfing[67] have explored the saddle point for H atom exchange. They find this saddle point is located 560 meV below $H + O_2$, and therefore it is accessible. Very recently, Walch and Duchovic[68] have extended calculations away from the minimum energy path and saddle points to provide a global representation of the potential energy surface. In addition, they report a new collinear saddle point.

Dynamic calculations are generally performed on analytical potential-energy surfaces generated from *ab initio* surfaces. Some of the analytical surfaces include many-body expansion (MBE) surfaces[69] and double many-body expansion (DMBE) surfaces.[70] A rather extensive list of references for both potential-energy surfaces and dynamic calculations on the HO_2 radical has been compiled by Varandas and co-workers.[71]

Two groups have performed dynamic calculations on the entrance channel $H + O_2$. In 1981, Miller[8] published both quasiclassical trajectory and quasiclassical quantum mechanical threshold calculations on the analytic representation given by Melius-Blint[9] of their *ab initio* calculations.

These results agreed with the early work of Schott[7] and highlighted the importance of a dynamic effect associated with a light particle reacting with two heavy particles. In Table III we compare our recommended rate coefficient with Miller's calculation. For the most accurate comparison we use the numbers given in Miller's later publication.[72] The results in Table II of Ref. 72 give a more accurate evaluation of the sums over vibrational and rotational quantum numbers.[73] These results agree with the measurements up to 1750 K, but then underestimate the rate coefficient at high temperatures. For example, at 2500 K, the calculation is 33% below our recommended value. This is approximately three standard deviations of either the experimental measurements or the Monte Carlo sampling uncertainty.

Since Miller's initial calculations, significant advances have occurred in both *ab initio* calculations of potential-energy surfaces and analytic representations of these surfaces for dynamic calculations. Very recently, Varandas, Brandão, and Pastrana[74] have utilized some of these advances and performed dynamic calculations on the double many-bodied expansion, DMBE IV, potential-energy surface of Pastrana *et al.*[67] Three types of dynamic calculations were performed: (1) quasiclassical trajectory (QCT), (2) quasiclassical trajectory-quantum mechanical threshold (QCT-QMT), and (3) quasiclassical trajectory-internal energy-quantum mechanical threshold (QCT-IEQMT). In the QCT-QMT method, only collisions with sufficient total energy to reach the zero-point energy of the products are integrated; all others are counted as nonreactive. In the QCT-IEQMT method, all trajectories that reach the products or recross back to reactants with less than the zero-point energy of the corresponding diatomic are discarded. These new results are also presented in Table III. Of these, the QCT and QCT-QMT approximations agree with the measurement up to 2500 K. At 3000 K, these calculations are approximately 15% below the measurements. Although the QCT-IEQMT method appears to be the most realistic approach for insuring that trajectory calculations properly account for the zero-point energy of the diatomic molecules, this method yields values significantly lower than the experimental results and close to the early calculations of Miller.[72]

We also note that Jacobs *et al.*[75] have recently measured the absolute reactive cross section for the $H + O_2$ reaction at 1.86 eV (21 600 K), 2.14 eV (24 800 K), and 2.57 eV (29 800 K). At the two lowest energies, their measured cross sections are a factor of 2 greater than Miller's calculated values[8] on the Melius-Blint[9] surface. For completeness, we point out that Bronikowski *et al.*[76] have also measured the dynamics of the $H + O_2$ reaction at a collision energy of 1.6 eV (18 600 K). Their data suggest that at this collision energy the reaction proceeds via two competing mechanisms: (1) a reaction involving a long-lived complex and (2) a direct reaction. Surely, reactive cross section measurements at much lower energies would provide a better test of calculations of the potential-energy surface, the reactive cross sections, and the mechanisms responsible for the reaction.

TABLE III. Comparison between measured and calculate rate coefficients for the reactions $H + O_2 \rightarrow OH + O$.

Temperature (K)	Measured ($\mu m^3 s^{-1}$)[c]	Miller[a] QCT-QMT	QCT	Varandas *et al.*[b] QCT-QMT	QCT-IEQMT
1000	0.092	0.087	···	0.099	0.0040
	0.015	0.012[e]		.016	.0010
1250	0.410[d]	0.452	···	···	···
	0.066	0.071			
1300	0.516	0.481	···	···	···
	0.052	0.041			
1750	2.26	1.98	2.62	2.21	1.43
	0.23	0.16	0.17	0.16	0.13
2000	3.86	3.05	4.75	4.23	3.01
	0.39	0.36	0.30	0.28	0.23
2500	8.15	5.46	7.79	7.31	5.71
	0.82	0.51	0.47	0.45	0.40
3000	13.4	···	11.66	11.16	9.15
	1.3		0.68	0.67	0.61

[a] Reference 72, Table II.
[b] Reference 74, Table I.
[c] $1\ \mu m^3 s^{-1} = 10^{-12}\ cm^3 s^{-1}$.
[d] The numbers below the rate coefficients represent 1-σ standard deviation of the measurements.
[e] The numbers below the rate coefficients represent 1-σ standard deviation of the Monte Carlo sampling uncertainty.

E. $OH+O \rightarrow H+O_2$ rate

Most of the recent dynamic calculations on the HO_2 system have been performed on the reverse channel, OH + O. This high level of interest stems from the fact that the O + OH reaction occurs on an almost barrierless potential-energy surface with a deep well and long-range electrostatic forces. Also, considerations of the reverse reaction remove the endothermic energy of the forward reaction and, thereby display the dynamic aspects more clearly. To compare calculations of the reverse rate to our results we calculated the equilibrium constant from the JANAF thermochemical data base[77] and used Eq. (12) to calculate the reverse rate coefficient from 1000 to 5000 K. To be complete we add the low temperature measurements of Lewis and Watson[78] and Howard and Smith.[79] The combined results for the reverse rate coefficient are shown as the solid line in Fig. 11. The rate coefficient reaches a minimum of $(1.58 \pm 0.16) \times 10^{-11}\ cm^3 s^{-1}$ at 2800 K and then rises slowly. At 5000 K it is $(1.64 \pm 0.16) \times 10^{-11}\ cm^3 s^{-1}$.

In 1986, Miller[72] published calculations of the rate coefficient for the reverse reaction. Again, he performed quasiclassical trajectory calculations on the Melius-Blint[9] surface. His results, from Table I of Ref. 72, are shown as the diamonds in Fig. 11. The standard deviation of the Monte Carlo sampling uncertainty is approximately 10% and is represented by the error bars. In this work, Miller pointed out that nonstatistical "recrossing" plays an important role in determining the rate coefficient. For example, at 2500 K, he found that 70% of the formed HO_2^* decays back to the entrance channel. His calculated value is 30% below our measurements at 2500 K.

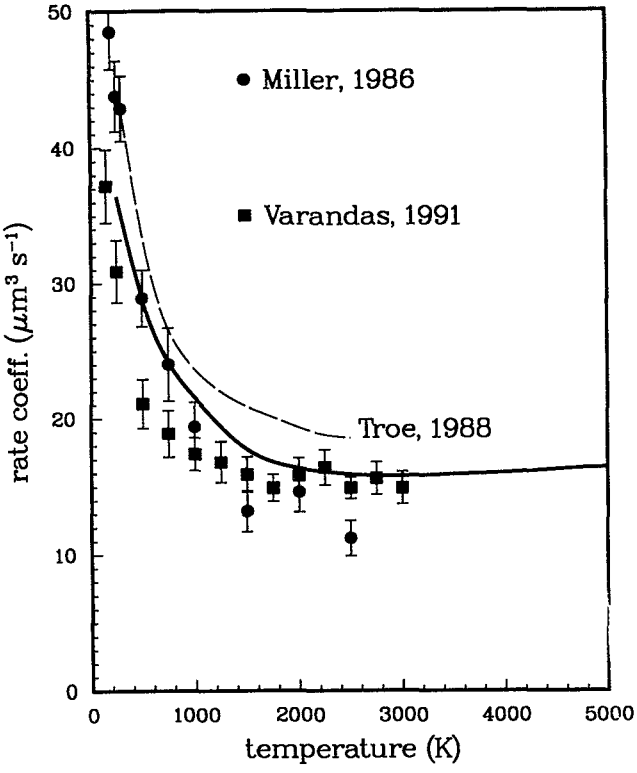

FIG. 11. Calculated rate for the reverse reaction $OH + O \rightarrow O_2 + H$. The solid line represent our recommended value calculated from the equilibrium constant. The calculations are from: ● Miller, Ref. 72, Table I; --- Troe, Ref. 80; and ■ Varandas *et al.*, Ref. 74, Table III. Note, $1\ \mu m^3\ s^{-1} = 10^{-12}$ $cm^3\ s^{-1}$. The error bars on the calculations represent one standard deviation of the Monte Carlo sampling uncertainty.

At about the same time as Miller performed scattering calculations, statistical adiabatic channel model calculations[12] on a simple short-range/long-range switching model for the radial and angular interaction potential were performed. More recently, Troe[80] has considered the HO_2^* complex as a "loose-entrance/loose-exit" system and discussed five levels of complexity in the calculation of the thermal rate coefficient: (1) phase-space theory with a long range OH + O interaction on the ground electronic potential-energy surface only, (2) phase-space theory with a more realistic short range potential, (3) the tightening of the activated complex via statistical adiabatic channel calculations of accurate channel eigenvalues, (4) statistical recrossing of the complex back to OH + O, and, finally, (5) contributions from the excited $^2A'$ electronic surface. Calculations at levels (1) and (2) produce nearly identical temperature-independent results up to 2500 K. Advances to levels (3) and (4) lower the rate coefficient by a factor between 2 and 3 and introduce a slight temperature dependence near 2500 K. Finally, the addition of contributions from the excited electronic surface significantly modifies the temperature dependence and reduces the magnitude of the rate coefficient by nearly a factor of 10 at 2500 K. These results are shown as the dashed line in Fig. 11. These calculations overestimate the rate coefficient by 17% at 2500 K.

Very recently, Varandas and his co-workers performed the same trajectory calculations discussed previously for the forward reaction. The results for the QCT-IEQMT approximation, Table III of Ref. 74 (of the three, this approximation agrees best with the measurements) are also shown as points in Fig. 11. We should point out, Nyman and Davidsson[81] have also performed QCT calculations on the same double many-body expansion potential-energy surface used by Varandas *et al.*,[82] DMBE III. Nyman and Davidsson found the recrossing factors depend critically on how the vibrational zero-point energy is treated. In addition, even when they treated the zero-point energy the same as Varandas *et al.*, the calculated thermally averaged rate coefficient was significantly lower. Nyman and Davidsson were unable to identify the source of this discrepancy. However, they did point out the need to calculate at least 1000 trajectories to obtain reasonable statistical uncertainties.

Before we draw any conclusions, we make the following observations. First, all trajectory and scattering calculations have been performed on the $^2A''$ ground surface of the hydroperoxyl radical, HO_2. This surface correlates to both bimolecular pairs $H(^2S) + O_2(^3\Sigma_g^+)$ and $O(^3P) + OH(^2\Pi_i)$. On the other hand, the initial reactants for the O + OH reaction also correlate with the first excited electronic surface of HO_2, $^2A'$, which correlates with the bimolecular pair $H(^2S) + O_2(^1\Delta_g)$. Therefore, the O + OH reaction can form both triplet and singlet molecular oxygen. Since the $H + O_2(^1\Delta_g, v = 0)$ level is 205 meV below the $O + OH(^2\Pi_i, v = 1)$ level, hydroxyl molecules in $v \geqslant 1$ have sufficient energy to create singlet oxygen. If we use the rule of thumb that all levels within 4 kT of the ground level should be considered when performing dynamic calculations, then the potential-energy surface leading to the creation of singlet oxygen should be considered for all temperatures above 1000 K. Lunt *et al.*[83] have already observed the formation of singlet O_2 by monitoring the near-infrared emission at 1.27 μm. Unfortunately, they were not able to extract a rate coefficient. Also, Holstein *et al.*[84] have observed $^2A'$ to $^2A''$ emission which they attribute to vibrationally excited HO_2 radicals formed during the thermal recombination of H atoms with O_2 at room temperature. This excitation may be due to vibrationally excited ground state molecules undergoing collision induced $V \rightarrow E$ energy transfer. Given these two experimental observations and Graff and Wanger's[85] and Troe's[86] recent calculations of a variety of crossing and avoided crossings on the fine structure of the potential-energy surface of OH + O, we must conclude that the excited surface can no longer be ignored in quasiclassical and quantum scattering calculations. Second, since the rates of the forward and reverse reactions only differ by a factor of 4 over the temperature range 2000 to 5000 K, the reverse reaction could be producing significant amounts of singlet oxygen in our experiment. Since singlet oxygen is metastable, spin selection rules prevent radiative transitions to the triplet ground state, and spin-changing collisions have vanishingly small cross sections, it will not decay to triplet oxygen, but will react with atomic hydrogen on the $^2A'$ surface. If singlet oxygen could be detected and its concentration measured in high-temperature shock tube experiments, this

observation would confirm the importance of the $^2A'$ surface. Therefore, we can identify at least two outstanding challenges. One, measurements of the singlet-to-triplet O_2 branching ratio as a function of temperature for the $O + OH \rightarrow H + O_2$ reaction would provide crucial information which could be used to test theoretical calculations. Two, calculations of the rate of both the forward and reverse reactions at high temperatures must include the $^2A'$ surface of the HO_2 radical. The fact that the reactions can take place on two different surfaces at high temperatures adds yet another interesting aspect to this important chemical system.

Therefore, we may conclude the following: (1) At the present time there are four sets of measurements of the rate of $H + O_2$ which agree to within experimental uncertainty. These experiments were performed in different laboratories, with different techniques, and under different experimental conditions. In spite of these differences, the results agree to within their respective experimental errors and when combined they produce a rate coefficient that has an experimental uncertainty of $\pm$ 10% over the temperature range 960 to 5300 K. The status of the experimental measurements of the rate coefficient for this important combustion system has significantly improved within the last year. (2) Some calculations of the rate coefficient agree with the measurements and others do not. From our point of view, there is enough ambiguity in the fundamental assumptions which define the trajectory calculation techniques (for example, the many different ways of treating the zero-point energy and the lack of agreement between calculated and thermodynamic equilibrium constants) that we cannot determine if agreement between experiment and theory is simply fortuitous and/or if disagreement indicates something fundamentally wrong with the approach. In addition, the proper way to treat multiple potential-energy surfaces has not been established. We hope that the significant extension of the temperature range provided by our experimental results and the high precision of these results will help resolve some of these issues.

ACKNOWLEDGMENTS

This work was supported by the U. S. Department of Energy, Office of Basic Energy Sciences, Division of Chemical Sciences. We thank J. V. Michael, P. J. Ogren, and A. F. Wagner for helpful discussions and comments on the manuscript. We thank A. J. C. Varandas for sharing with us his preliminary calculations. R. J. Kee, F. M. Rupley, and A. K. Lutz provided support for the computer codes from Sandia. We thank D. R. Crosley, N. Fujii, R. K. Hanson, J. V. Michael, K. S. Shin, and A. J. C. Varandas for making available manuscripts prior to publication. Work performed under the auspices of the U. S. Department of Energy, Office of Energy Research, Division of Chemical Sciences.

[1] J. N. Bradley, *Flame and Combustion Phenomena* (Methuen, London, 1969), and references therein.
[2] C. K. Westbrook and F. L. Dryer, Prog. Energy Combust. Sci. **10**, 1 (1984), and references therein.
[3] G. Dixon-Lewis, in *Combustion Chemistry*, edited by W. C. Gardiner, Jr. (Springer, New York, 1984), pp. 21–125.
[4] D. L. Baulch, D. D. Drysdale, D. G. Horne, and A. C. Lloyd, *Evaluated Data for High Temperature Reactions* (Butterworths, London, 1972), Vol. 1; D. L. Baulch, R. A. Cox, P. J. Crutzen, R. F. Hampson, J. A. Kerr, and R. T. Watson, J. Chem. Ref. Data **11**, 327 (1982).
[5] N. Cohen and K. R. Westberg, J. Phys. Chem. Ref. Data **12**, 531 (1983).
[6] J. Warnatz, in *Combustion Chemistry*, edited by W. C. Gardiner, Jr. (Springer, New York, 1984), pp. 197–360.
[7] G. L. Schott, Combust. Flame **13**, 357 (1973).
[8] J. A. Miller, J. Chem. Phys. **74**, 5120 (1981).
[9] C. F. Melius and R. J. Blint, Chem. Phys. Lett. **64**, 183 (1979).
[10] P. Frank and T. Just, Ber. Bunsenges. Phys. Chem. **89**, 181 (1985).
[11] A. L. Myerson, H. M. Thompson, and W. S. Watt, J. Phys. Chem. **42**, 3331 (1965); and A. L. Meyerson and W. S. Watt, J. Chem. Phys. **49**, 425 (1968).
[12] C. J. Cobos, H. Hippler, and J. Troe, J. Phys. Chem. **89**, 342 (1985); and J. Troe, *ibid.* **90**, 3485 (1986).
[13] L. A. M. Quintales, A. J. C. Varandas, and J. M. Alvariño, J. Phys. Chem. **92**, 4552 (1988).
[14] R. K. Hanson, S. Salimain, G. Kychakoff, and R. A. Booman, Appl. Opt. **22**, 641 (1983).
[15] N. Fujii and K. S. Shin, Chem. Phys. Lett. **151**, 461 (1988); and N. Fujii, T. Sato, H. Miyama, K. S. Shin, and W. C. Gardiner, Jr., in *Seventeenth International Symposium on Shock Waves and Shock Tubes*, edited by Y. W. Kim (American Institute of Physics, New York, 1989).
[16] D. A. Masten, R. K. Hanson, and C. T. Bowman, J. Phys. Chem. **94**, 7119 (1990).
[17] T. Yuan, C. Wang, C.-L. Yu, M. Frenklach, and M. J. Rabinowitz, J. Phys. Chem. **95**, 1258 (1991).
[18] A. N. Pirraglia, J. V. Michael, J. W. Sutherland, and R. B. Klemm, J. Phys. Chem. **93**, 282 (1989).
[19] K. S. Shin and J. V. Michael, J. Chem. Phys. **95**, 262 (1991).
[20] G. Burns and D. F. Hornig, Can. J. Chem. **38**, 1702 (1960).
[21] W. A. VonDrasek, S. Okajima, J. H. Kiefer, P. J. Ogren, and J. P. Hessler, Appl. Opt. **29**, 4899 (1990).
[22] J. A. Miller and C. T. Bowman, Prog. Energy Combust. Sci. **15**, 287 (1989).
[23] M. J. Pilling, in *Modern Gas Kinetics Theory, Experiment, and Application*, edited by M. J. Pilling and I. W. M. Smith (Blackwell Scientific, Oxford, 1987), pp. 303–315.
[24] A. E. Lutz, R. J. Kee, and J. A. Miller, *SENKIN: A Fortran Program for Predicting Homogeneous Gas Phase Chemical Kinetics With Sensitivity Analysis*, Sandia Report No. SAND87-8248, December 1989.
[25] M. Keiffer, A. J. Miscampbell, and M. J. Pilling, J. Chem. Soc. Faraday Trans. 2 **84**, 505 (1988).
[26] P. D. Bevington, *Data Reduction and Error Analysis for the Physical Sciences* (McGraw-Hill, New York, 1969).
[27] C. Daniel and F. S. Wood, *Fitting Equations to Data* (Wiley, New York, 1980).
[28] B. R. Martin, *Statistics for Physicists* (Academic, London 1971), pp. 30–35.
[29] M. Lampton, M. Margon, and S. Bowyer, Astrophys. J. **208**, 177 (1976).
[30] R. E. Mitchell and R. J. Kee, *A General-Purpose Computer Code for Predicting Chemical Kinetic Behavior Behind Incident and Reflected Shocks*, Sandia Report No. SAND82-8205, March 1982.
[31] R. J. Kee, F. M. Rupley, and J. A. Miller, *Chemkin-II: A Fortran Chemical Kinetics Package for the Analysis of Gas-Phase Chemical Kinetics*, Sandia Report No. SAND89-8009 ● UC-401, September 1989.
[32] R. J. Kee, F. M. Rupley, and J. A. Miller, *The CHEMKIN Thermodynamic Data Base*, Sandia Report No. SAND87-8215 ● UC-4, April 1989.
[33] E. F. Greene and J. P. Toennies, *Chemical Reactions in Shock Waves* (Edward Arnold, London, 1964), p. 87.
[34] A. Goldman and J. R. Gillis, J. Quant. Spectrosc. Radiat. Transfer **25**, 111 (1981).
[35] E. C. Rea, Jr., A. Y. Chang, and R. K. Hanson, J. Quant. Spectrosc. Radiat. Transfer **37**, 117 (1987); **41**, 29 (1989).
[36] E. F. Green and J. P. Toennies, *Chemical Reactions in Shock Waves* (Edward Arnold, London, 1964), pp. 21–22.
[37] F. E. Belles and T. A. Brabs, *Thirteenth Symposium (International) on Combustion* (The Combustion Institute, Pittsburgh, 1971), p. 165.
[38] A. E. Siegman, *Lasers* (University Science Books, Mill Valley, 1986), p. 636.
[39] S. L. Meyer, *Data Analysis for Scientists and Engineers* (Wiley, New York, 1975), pp 359–386.
[40] H. O. Pritchard, *The Quantum Theory of Unimolecular Reactions* (Cam-

bridge University, Cambridge, 1984), p. 116. Some authors have used the adjective "induction" to describe this effect. Unfortunately, the term induction has also been used to describe ignition delay times, i.e., the time at which the concentration of a species reaches some arbitrary value. For a discussion of ignition delay times see, W. Tsang and A. Lifshitz, Annu. Rev. Phys. Chem. **41**, 559 (1990). Therefore, to avoid misunderstanding, we shall use the adjective incubation.

[41] K. L. Wray, J. Chem. Phys. **37**, 1254 (1962); W. S. Watt and A. L. Myerson, *ibid.* **51**, 1638 (1969); and W. D. Breshears, P. F. Bird, and J. H. Kiefer, *ibid.* **55**, 4017 (1971).

[42] J. E. Dove, W. S. Nip, and H. Teitelbaum, in *Fifteenth Symposium (International) on Combustion* (The Combustion Institute, Pittsburg, 1974), p. 903.

[43] E. A. Dorko, R. W. Crossley, U. W. Grimm, G. W. Mueller, and K. Scheller, J. Phys. Chem. **77**, 143 (1973).

[44] A. P. Penner and W. Forst, J. Chem. Phys. **67**, 5296 (1977); and W. Forst and A. P. Penner, *ibid.* **72**, 1435 (1980).

[45] W. Forst, J. Phys. Chem. **84**, 3050 (1980).

[46] J. Troe, J. Chem. Phys. **66**, 4745 (1977); **77**, 3485 (1982); N. Snider, *ibid.* **85**, 4207 (1986).

[47] J. E. Dove and H. Teitelbaum, Chem. Phys. **6**, 431 (1974).

[48] M. Camac, J. Chem. Phys. **34**, 448 (1961).

[49] D. R. White and R. C. Millikan, J. Chem. Phys. **39**, 2107 (1963).

[50] R. C. Millikan and D. R. White, J. Chem. Phys. **39**, 3209 (1963).

[51] V. Subba Rao and G. B. Skinner, J. Chem. Phys. **81**, 775 (1984).

[52] E. W. Montroll and K. E. Shuler, J. Chem. Phys. **26**, 454 (1957).

[53] D. R. Crosley, K. J. Rensberger, and J. B. Jeffries, in *Advances in Laser Science IV*, edited by J. L. Gole, D. F. Heller, M. Lapp, and W. C. Stwally, Conf. Proc. Vol. 191 (American Institute of Physics, New York, 1989), p. 615.

[54] G. P. Glass, H. Endo, and B. K. Chaturvedi, J. Chem. Phys. **77**, 5450 (1982).

[55] K. J. Rensberg, J. B. Jeffries, and D. R. Crosley, J. Chem. Phys. **90**, 2174 (1989); and G. A. Raiche, J. B. Jeffries, K. J. Rensberg, and D. R. Crosley, *ibid.* **92**, 7258 (1990).

[56] J. E. Spencer and G. P. Glass, Chem. Phys. **15**, 35 (1976).

[57] J. E. Spencer, H. Endo, and G. P. Glass, *Sixteenth Symposium (International) on Combustion* (The Combustion Institute, Pittsburg, 1976), p. 829.

[58] K. Kleinermanns and R. Schinke, J. Chem. Phys. **80**, 1440 (1984).

[59] J. P. Rink, J. Chem. Phys. **36**, 262 (1962).

[60] K. P. Huber and G. Herzberg, *Molecular Spectra and Molecular Structure IV. Constants of Diatomic Molecules* (Van Nostrand Reinhold, New York), 1979.

[61] H. E. Hunziker and H. R. Wendt, J. Chem. Phys. **60**, 4622 (1974).

[62] K. H. Becker, E. H. Fink, P. Langen, and U. Schurath, J. Chem. Phys. **60**, 4623 (1974).

[63] E. R. Fisher and P. B. Armentrout, J. Phys. Chem. **94**, 4396 (1990).

[64] S. R. Langhoff and R. L. Jaffe, J. Chem. Phys. **71**, 1475 (1979).

[65] T. H. Dunning, Jr., S. P. Walch, and M. M. Goodgame, J. Chem. Phys. **74**, 3482 (1981).

[66] S. P. Walch, C. M. Rohlfing, C. F. Melius, and C. W. Bauschlicher, Jr., J. Chem. Phys. **88**, 6273 (1988).

[67] S. P. Walch and C. M. Rohlfing, J. Chem. Phys. **91**, 2372 (1989).

[68] S. P. Walch and R. J. Duchovic, J. Chem. Phys. **94**, 7068 (1991).

[69] S. Farantos, E. C. Leisegang, J. N. Murrell, K. Sorbie, J. J. C. Teixeira-Dias, and A. J. C. Varandas, Mol. Phys. **34**, 947 (1977).

[70] A. J. C. Varandas, Mol. Phys. **53**, 1303 (1984).

[71] M. R. Pastrana, L. A. M. Quintales, J. Brandão, and A. J. C. Varandas, J. Phys. Chem. **94**, 8073 (1990).

[72] J. A. Miller, J. Chem. Phys. **84**, 6170 (1986).

[73] J. A. Miller (private communication, 9 July 1991).

[74] A. J. C. Varandas, J. Brandão, and M. R. Pastrana, J. Chem. Phys. (submitted).

[75] A. Jacobs, F. M. Schuler, H. R. Volpp, M. Wahl, and J. Wolfrum, Ber. Bunsenges. Phys. Chem. **94**, 1390 (1990); and A. Jacobs, H. R. Volpp, and J. Wolfrum, Chem. Phys. Lett. **177**, 200 (1991).

[76] M. J. Bronikowski, R. Zhang, D. J. Rakestraw, and R. N. Zare, Chem. Phys. Lett. **156**, 7 (1989).

[77] M. W. Chase, Jr., C. A. Davies, J. R. Downey, Jr., D. J. Frurip, R. A. McDonald, and A. N. Syverud, J. Phys. Chem. Ref. Data **14**, Suppl. No. 1, (1985); *JANAF Thermochemical Table*, 3rd ed., edited by D. R. Lide, Jr. (American Institute of Physics, New York, 1985.)

[78] R. S. Lewis and R. T. Watson, J. Phys. Chem. **84**, 3495 (1980).

[79] M. J. Howard and I. W. Smith, J. Chem. Soc. Faraday 2 **77**, 997 (1981).

[80] J. Troe, *Twenty-Second Symposium (International) on Combustion* (The Combustion Institute, Pittsburg, 1988), pp. 843–862.

[81] G. Nyman and J. Davidsson, J. Chem. Phys. **92**, 2415 (1990).

[82] A. J. C. Varandas, J. Brandão, and L. A. M. Quintales, J. Phys. Chem. **92**, 3732 (1988).

[83] S. T. Lunt, G. Marston, and R. P. Wayne, J. Chem. Soc. Faraday Trans. 2 **84**, 899 (1988).

[84] K. J. Holstein, E. H. Fink, J. Wildt, R. Winter, and F. Zabel, J. Phys. Chem. **87**, 3943 (1983).

[85] M. M. Graff and A. F. Wagner, J. Chem. Phys. **92**, 2423 (1990).

[86] J. Troe, Ber. Bunsenges. Phys. Chem. **94**, 1183 (1990).